HHS Public Access

Author manuscript

Neurobiol Dis. Author manuscript; available in PMC 2017 May 01.

Published in final edited form as:

Neurobiol Dis. 2016 May ; 89: 76–87. doi:10.1016/j.nbd.2016.02.006.

Neuron class-specific requirements for Fragile X Mental Retardation Protein in critical period development of calcium signaling in learning and memory circuitry

Caleb A. Doll and **Kendal Broadie**

Department of Biological Sciences, Department of Cell and Developmental Biology, The Vanderbilt Kennedy Center for Research on Human Development, Vanderbilt University and Medical Center, Nashville, TN, 37235 USA

Graphical Abstract

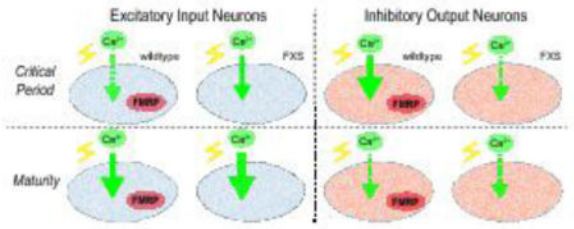

Introduction

Fragile X syndrome (FXS) is the leading heritable cause of intellectual disability (Boyle and Kaufmann, 2010) and most prevalent single-gene autism spectrum disorder (Wang et al., 2012). The disease state is caused by lack of Fragile X Mental Retardation Protein (FMRP), a key regulator of activity-dependent neural circuit modulation during critical period development (Doll and Broadie, 2014). The full range of FMRP function is broad and inconclusive, but includes regulation of multiple classes of voltage-gated ion channels, via both RNA-binding translational control (Gross et al., 2011; Lee et al., 2011; Strumbos et al., 2010) and direct channel-binding interactions (Brown et al., 2010; Deng et al., 2013; Ferron et al., 2014; Zhang et al., 2014). Downstream, FMRP also regulates numerous calcium-binding proteins (CaBPs) involved in activity-dependent calcium signaling (Chen et al., 2003; Tessier and Broadie, 2011; Wang et al., 2009). Consistently, FXS disease models exhibit increased excitatory neurotransmission (Deng et al., 2013; Deng et al., 2011; Gibson

Corresponding author: Kendal Broadie, VU Station B, Box 35-1634, Nashville, Tennessee 37235-1634, USA Phone: (615) 936-3937, Fax: (615) 936-0129, kendal.broadie@vanderbilt.edu.

Conflict of interest: The authors declare no competing financial interests.

Author Contributions: C.A.D. and K.B. conceived and designed the experiments. C.A.D. performed all experiments and analyzed all data. C.A.D. and K.B. co-wrote the paper.

et al., 2008), defects in action potential termination (Brown et al., 2010; Deng et al., 2013; Zhang et al., 2012) and altered depolarization-triggered calcium influx (Deng et al., 2013; Deng et al., 2011; Ferron et al., 2014; Patel et al., 2013; Tessier and Broadie, 2011). Earlier work has elegantly mapped critical period functional refinement (Meredith, 2015), and defining FMRP roles in these activity-dependent mechanisms at single cell resolution during critical periods is now possible through the application of incisive *Drosophila* genetics.

The *Drosophila* FXS disease model has long been instrumental in dissecting developmental and activity-dependent FMRP roles (Doll and Broadie, 2015; Gatto and Broadie, 2008; Pan et al., 2004; Tessier and Broadie, 2008; Weisz et al., 2015; Zhang et al., 2001). Our past studies have identified hyper-excitability, calcium influx and store release defects, and changes in CaBP expression in the absence of FMRP function (Gatto and Broadie, 2008; Repicky and Broadie, 2009; Tessier and Broadie, 2008; Tessier and Broadie, 2011). During development of the well-mapped Mushroom body (MB) learning/memory circuit, we recently identified activity-dependent and FMRP-dependent changes in synaptic connectivity coincident with the early-use sensory input critical period that occurs immediately following eclosion (Doll and Broadie, 2015). Individually identified single cells of opposing excitatory input and inhibitory output neuron classes exhibit opposite activity-dependent responses to optogenetic stimulation and hyperpolarization, effects that require FMRP specifically during this critical period.

The present study investigates the neuron class-specific FMRP functional requirements in excitatory vs. inhibitory neurons in calcium signaling dynamics during MB critical period circuit development (Kaeser and Regehr, 2014). Our working hypothesis at the onset of this study was that FMRP regulates Ca^{2+} signaling dynamics in a cell type-specific manner in excitatory vs. inhibitory neurons, with a heightened requirement during the early-use MB critical period immediately following eclosion. The sophisticated *Drosophila* genetic toolkit is especially well suited for this cell-specific and developmental stage-specific dissection through the application of new highly-targeted neuronal transgenic drivers and conditional genetic manipulations. Our goal in this study was to elucidate the functional differences underlying activity-dependent development of these two distinct excitatory vs. inhibitory neuron types, utilizing calcium imaging within the *Drosophila* learning/memory circuit (Tomchik and Davis, 2009).

We focused on two MB extrinsic neurons; excitatory cholinergic input AL-mPN2 (Ito et al., 2014) and inhibitory GABAergic output MBON-γ1pedc>α/β (Aso et al., 2014b). We find that FMRP regulates calcium signaling dynamics in these two neuron classes in an opposite manner during early-use critical period development. In cholinergic projection neurons carrying excitatory input from olfactory antennal lobe to MB calyx (Iniguez et al., 2013), FMRP absence leads to elevated calcium transients only during the critical period. In contrast, the MBON-11 GABAergic output neurons, which are postsynaptic to Kenyon Cells at the MB spur (Tanaka et al., 2008), display reduced calcium transients in *dfmr1* null mutants, but also only during the critical period. Cell autonomous rescue and knockdown demonstrate a specific critical period FMRP requirement in both neuron classes. Cell autonomous optogenetic stimulation during the critical period causes heightened activity-dependent calcium transients, indicating that critical period activity modulates subsequent

excitability. Importantly, heightened critical period activity in excitatory neurons induced calcium signaling dynamics strikingly reminiscent of FXS, supporting the hyperexcitation theory of FXS and providing a developmental mechanism for the excitation/inhibition imbalance characterizing the disease state (Gatto and Broadie, 2010). These results demonstrate neuron class-specific functional roles for FMRP restricted to critical period development.

Materials & Methods

Drosophila genetics

All stocks were reared on standard cornmeal/agar/molasses food at 25°C unless stated otherwise. Multiple recombinant lines of *dfmr1* null allele $dfmr1^{50M}$ (Zhang et al., 2001) were generated with standard genetic techniques using a combination of the following transgenic lines; 1) R12G04-Gal4, R65G01-Gal4, 20XUAS-IVS-GCamp5G and tubP-Gal80[ts];TM2/TM6 from the *Drosophila* Stock Center (Bloomington, IN, USA), 2) UAS-*dfmr1*-RNAi (TRiP, Harvard) and 3) UAS-ChR2(H134R)-mCherry generously provided by Leslie Griffith (Pulver et al., 2009). For conditional Gal80ts *dfmr1*-RNAi and wildtype *dfmr1*-rescue (UAS-9557-3, wildtype *dfmr1* under UAS control; Gatto and Broadie, 2009) experiments, both controls and experimental animals were raised at permissive 18°C (Gal80ts active) until the last pupal day (P4), and then shifted to restrictive 29°C (Gal80ts inactive) until 1 day post-eclosion (dpe).

Immunocytochemistry and imaging

Immunocytochemistry was carried out as previously described (Doll and Broadie, 2015). Primary rabbit anti-GFP (ab290; Abcam, Cambridge, UK) was used at a 1:2000 dilution, and secondary antibody anti-mouse-IgG AlexaFluor 488 (Molecular Probes, Eugene, OR) was used at a 1:500 dilution. Images were acquired for the central brain region on a Zeiss Meta 510 confocal microscope with 40-100X objectives, and collected as Z-stacks of 1μm section depth.

Calcium imaging

The 20XUAS-IVS-GCamp5G line (Bloomington stock center #42037) was used as a transgenic [Ca^{2+}] reporter (Akerboom et al., 2012). This reporter was crossed to R12G04-Gal4 and R65G01-Gal4 driver lines in both w^{1118} genetic background control and *dfmr1* null mutant backgrounds. Acutely dissected brains from all four genotypes were immobilized on 30 mm petri dishes in 3 mL of physiological saline containing 128 mM NaCl, 2 mM KCl, 4 mM $MgCl_2$, 35.5 mM sucrose, 5 mM Hepes, and 1.8 mM Ca^{2+}, pH 7.2 (Tessier and Broadie, 2011). Labeled cell soma were immediately imaged with a 40x water-immersion objective with maximal pinhole aperture on a Zeiss LSM510Meta laser-scanning confocal microscope. Each neuron was outlined using a region of interest (ROI) box, and a time series was captured at 128x128 resolution at maximum scanning speeds (44ms/frame). Baseline fluorescence was determined for each selected neuron (~350 frames/15 sec), followed by acute K^+ depolarization (60 mM KCl) (Gatto et al., 2014) with recording for 2500 total frames (110 secs). ImageJ was used for image registration and determination of baseline fluorescence intensity values within the ROI (Schneider et al., 2012). Baseline

fluorescence was defined from a 20-frame average that occurred in the 5 seconds prior to the onset of transient initiation and was used to normalize the data set. Data were plotted as the relative change in fluorescence from baseline divided by the baseline ($\Delta F/F$; $(F_{t1} - F_{baseline})/F_{baseline}$), with each data point representing an average and standard error of 20 frames. Line graph data points represent an average of 20 frames (captured at 44 ms/frame), therefore every data point represents 880 ms. Only one calcium transient was captured from each individual neuron, and only one neuron was analyzed from each animal. Time to peak $[Ca^{2+}]$ was calculated by averaging raw individual trace data, locating the frame with the greatest fluorescence value in each trial, relative to the initiation of the transient (in seconds: frame # x 0.0044 s). Average peak fluorescence values compare the maximum 20 frame fluorescent values from each group of transient initiation-aligned traces. Only individual traces with half-life decay functions in which $r^2 > 0.9$ were included in decay analyses. Decay half-life ($t_{1/2}$) was estimated using the least-squares method to fit the 20% to 80% decay fluorescence to a single-exponential function $Y=Y_0e^{-kt}$ where $t_{1/2}=\ln 2/k$ in MATLAB (version R2012b, Mathworks, Natick, MA).

Optogenetics

Transgenic animals were generated from pairwise crosses between the UAS-ChR2(H134R)-mCherry optogenetic channel line and 1 of 2 drivers (R12G04-Gal4 or R65G01-Gal4), both in w^{1118} genetic background control and *dfmr1* null mutant backgrounds. Offspring from all four genotypes were fed from hatching on standard food supplemented with either 10μL EtOH (in 10 ml volume; vehicle control) or 100μM all-trans retinal (ATR), an essential co-factor for channelrhodopsin function (Ataman et al., 2008). Upon eclosion, developmentally staged animals were placed in 30mm petri dishes with Watman paper strips saturated in a 20% sucrose solution containing either the vehicle control or 100μM ATR. All control and experimental animals were placed in a LED exposure chamber with two 470nm blue light Luxeon Rebel Endor Star 3X 15-Watt LED arrays (LED Supply, Randolph, VT). At 15V, the LED arrays generate ~100 $\mu W/cm^2$ of blue light at the working distance of 2cm. Animals were exposed to 24 hrs of 20ms light pulses at 5Hz frequency. Brains from light-exposed animals then underwent Ca^{2+} imaging as described above.

Statistics

All statistical analyses were performed using Instat or Prism (GraphPad Software, San Diego, CA). Data from two group comparisons were analyzed with a two-tailed unpaired *t*-test. Data from three group or more comparisons were analyzed with one-way analysis of variance (ANOVA) and Dunnett post hoc tests were applied to compare individual experimental groups to control (*F* and *p* values reported). Transient initiation-aligned traces (mean ± standard error) for each genotype are presented in line graphs. Data are presented in box-and-whisker plots (minimum, median, maximum and quartiles). Sample size definitions for peak amplitude, time to peak amplitude and decay half-life, *n* = number of individual transient recordings (1 transient per neuron, per animal). Significance levels in figures are represented as $p>0.05$ (not significant, n.s.), $p<0.05$ (*), $p<0.01$ (**) and $p<0.001$ (***).

Results

FMRP-defined critical period development in excitatory vs. inhibitory MB circuit neurons

FMRP shows a tight peak of expression from the last day of pupal development (P4) though the first day post-eclosion (1 dpe) that defines an early-use critical period of activity-dependent neural circuit refinement (Fig. 1A; Tessier and Broadie, 2008; Tessier and Broadie, 2012). Following this window, FMRP levels rapidly fall to much lower steady-state expression in the mature brain (e.g. 7 dpe; Fig. 1A). Our recent work revealed a restricted temporal FMRP requirement in the development of MB synaptic connectivity during this critical period, with opposite activity-dependent directionality in two opposite classes of MB extrinsic neurons; an excitatory input neuron and an inhibitory output neuron (Fig. 1B; Doll and Broadie, 2015). To test for the functional mechanism, we assayed activity-dependent Ca^{2+} dynamics in these two distinctive excitatory vs. inhibitory neuron classes, focusing on the FMRP-defined, early-use critical period window (P4 – 1 dpe) compared to adult maturity (7 dpe; Fig. 1A).

The highly restricted R65G01-Gal4 (*Leonardo*/14-3-3δ gene) FlyLight transgenic driver specifically targets the excitatory cholinergic MB input neuron (antennal lobe medial projection neuron 2: AL-mPN2), allowing single-cell resolution recording and manipulation (Fig. 1B; Doll and Broadie, 2015; Jenett et al., 2012). mPN2 cell bodies are located at the ventrolateral edge of the central brain in the subesophogeal zone (SEZ; Ito et al., 2014), with a primary process that travels medially before bifurcation into a collateral and a dorsal branch (Fig. 1B; Tanaka et al., 2012). mPN2 is characterized as a bilateral uniglomerular medial antennal lobe tract (mALT) projection neuron with a dendritic arbor specific to the VL1 glomerulus of the antennal lobe (AL; Fig. 1B2). The axon travels through the mALT, with primary presynaptic outputs to 3–5 microglomeruli in the MB calyx on Kenyon Cells (KCs) as well as further axon terminals in the lateral horn (LH; Fig. 1B3).

The R12G04-Gal4 (Oli gene) FlyLight driver specifically targets the inhibitory GABAergic output neuron MBON-γ1pedc>α/β (abbreviated MBON-11; Aso et al., 2014b), formerly identified as MB-MVP2 (Fig 1B; Aso et al., 2014b; Doll and Broadie, 2015; Jenett et al., 2012). Single MBON-11 neuronal cell bodies are located in the inferiormedial protocerebrum (IPm) in the anterior portion of the central brain, with a prominent dendritic arbor within the MB spur (Fig. 1B1), and an output axon that bifurcates into collateral and vertical branches (Tanaka et al., 2008). These GABAergic MB output neurons are required in multiple sensory modalities (both olfactory and visual) for aversive memory consolidation (Aso et al., 2014b). Our previous work established a tight temporal requirement for FMRP function during the early sensory input critical period in the activity-dependent development of both mPN2 and MBON-11 dendritic arborization (Doll and Broadie, 2015).

Excitatory mPN2 displays an FMRP-dependent developmental shift in Ca^{2+} dynamics

The FMRP-dependent refinement of MB circuitry is confined to a transient window of development during early sensory use, immediately following eclosion (Doll and Broadie, 2015; Tessier and Broadie, 2008), similar to a comparable requirement in mammals (Portera-Cailliau, 2012). Based on our previous studies, we focused analyses on the 1 dpe

critical period compared to the 7 dpe time point representing adult maturity. The GCamp5G transgenic [Ca^{2+}] reporter (Akerboom et al., 2012) was used to assay activity-dependent Ca^{2+} signaling dynamics in single, individually identified mPN2 and MBON-11 neuronal soma as a function of development time in w^{1118} genetic background control compared to *dfmr1* null mutants. Neurons were imaged to establish baseline GCamp5G fluorescence (1.8mM extracellular bath [Ca^{2+}]) and then acutely depolarized with high [K^+] (60mM KCl) to generate optically measurable Ca^{2+} transients (Fiala and Spall, 2003). Three primary parameters were used to measure the Ca^{2+} transients: time to peak fluorescence (sec), peak fluorescence intensity and the half-life of transient termination (sec).

A summary of excitatory mPN2 neuron Ca^{2+} signaling dynamics at the 1 dpe critical period and at 7 dpe maturity is shown in Figure 2. At 1 dpe, UAS-GCamp5G driven by R65G01-Gal4 provides clear fluorescent Ca^{2+} reporter transients upon acute K^+ depolarization, which display a rapid rise to peak and slower decay (Fig. 2A). Compared to genetic background controls, *dfmr1* null mPN2 neurons exhibit a >35% increase in the Ca^{2+} transient peak (control, 0.29 ± 0.04, *n*=19 neurons; *dfmr1*, 0.46 ± 0.07, *n*=17 neurons, *t*-test, *p*=1.25E-20; Fig. 2A). Despite this greatly increased peak amplitude, the time to peak is comparable between genotypes (control, 9.16 ± 0.98 sec, *n*=19; *dfmr1*, 10.61 ± 1.20 sec, *n*=17, *t*-test, *p*=0.35). Similarly, both wildtype and *dfmr1* null mPN2 neurons display comparable slow Ca^{2+} transient decay properties (control $t_{1/2}$, 37.44 ± 5.52 sec, r^2=0.96 ± 0.01, *n*=19; *dfmr1* $t_{1/2}$, 40.82 ± 6.82, r^2=0.96 ± 0.01, *n*=17, *p*=0.70; Fig. 2A, bottom). These data show that FMRP limits the level of depolarization-induced Ca^{2+} signaling in mPN2 neurons, but does not impact the rate of Ca^{2+} clearance. Therefore, the extended calcium signaling profile in *dfmr1* nulls (extended return to baseline; Fig. 2A) is likely rooted in elevated influx capacity and not decay properties.

At maturity (7 dpe), depolarization-induced Ca^{2+} transients in excitatory mPN2 neurons have increased dramatically in wildtype (compare Figs. 2A and 2B). In contrast, the developmental change in *dfmr1* null mutants is blunted, with a much smaller increase in Ca^{2+} transient amplitude. As a result, depolarization-induced Ca^{2+} transients at 7 dpe are largely indistinguishable between wildtype and *dfmr1* null mPN2 neurons (Fig. 2B). Interestingly, at maturity the peak fluorescent amplitude is actually moderately reduced (~19%) in *dfmr1* nulls (0.69 ± 0.10, *n*=18 neurons) compared to controls (0.85 ± 0.08, *n*=22 neurons, *t*-test, *p*=1.02E-08; Fig. 2B), underscoring the dramatic developmental shift in wildtype Ca^{2+} signaling dynamics. The temporal Ca^{2+} transient characteristics in both control and mutant genotypes are comparable at maturity, including time to peak (control, 6.77 ± 0.55 sec, *n*=22; *dfmr1*, 7.57 ± 0.45 sec, *n*=18, *t*-test, *p*=0.29, n.s.; Fig. 2B), and decay half-life (control $t_{1/2}$, 20.23 ± 2.85 sec, r^2=0.97 ± 0.02, *n*=20; *dfmr1* $t_{1/2}$, 33.89 ± 8.85, r^2=0.92 ± 0.02, *n*=17, *t*-test, *p*=0.13, n.s.; Fig. 2B). These results suggest a restricted critical period requirement for FMRP in depolarization-induced Ca^{2+} signaling, with wildtype undergoing a dramatic developmental shift compared to *dfmr1* null mPN2 neurons, establishing comparable functional properties at maturity.

Inhibitory MBON-11 neurons show the opposite developmental shift in Ca^{2+} dynamics

Despite similar dendritic arbor architectural phenotypes, excitatory mPN2 and inhibitory MBON-11 neurons exhibit opposite FMRP-dependent responses to activity during critical period development (Doll and Broadie, 2015). Consistently, the functional Ca^{2+} signaling dynamics of these two neuron classes also display an opposite critical period specific shift in *dfmr1* mutants. At the 1 dpe critical period, acute depolarization of wildtype MBON-11 neurons causes a rapid rise to peak [Ca^{2+}] and a quick decay back to baseline (Fig. 3A). In *dfmr1* nulls, however, the 1 dpe Ca^{2+} transient peak is very significantly reduced in MBON-11 neurons (0.71 ± 0.08, *n*=20 neurons) compared to controls (1.29 ± 0.14, *n*=15 neurons, *t*-test, *p*=3.95E-53; Fig. 3A). Moreover, the time to peak is significantly longer in *dfmr1* null neurons (9.81 ± 0.89 sec, *n*=15) compared to controls (6.28 ± 0.80 sec, *n*=20, *t*-test, *p*=0.007; Fig. 3A, bottom), although the Ca^{2+} transient decay half-life is comparable between genotypes (control $t_{1/2}$, 7.22 ± 1.8, r^2=0.95 ± 0.01, *n*=20; null $t_{1/2}$, 9.07 ± 1.4 sec, r^2=0.94 ± 0.01, *n*=15, *t*-test, *p*=0.41, n.s.). The critical period reduction in Ca^{2+} transients in *dfmr1* null MBON-11 GABAergic neurons contrasts sharply with the elevation in *dfmr1* null mPN2 cholinergic neurons, showing a clear distinction between inhibitory and excitatory neurons in the developing MB circuit.

At maturity (7 dpe), wildtype MBON-11 neurons show a clear shift in Ca^{2+} transient peak fluorescence (0.81 ± 0.11, *n*=22 neurons), as they undergo a prominent decrease from the developmental critical period to adulthood (compare Figs. 3A and 3B). In contrast to the genetic background control, *dfmr1* null MBON-11 neurons retain remarkably similar activity-dependent Ca^{2+} signaling dynamics at maturity compared to the 1 dpe critical period (compare Figs. 3A and 3B). As in mPN2 neurons, the *dfmr1* null peak transient amplitude (0.83 ± 0.10, *n*=23 neurons, *t*-test: *p*=0.55) and time to peak (6.40 ± 0.57 sec, *n*=23, *t*-test: *p*=0.81) in inhibitory MBON-11 neurons were both indistinguishable from controls at maturity (Fig. 3B). The only *dfmr1* phenotype remaining at maturity is a significant increase in decay half-life compared to controls (5.88 ± 0.48 sec, r^2=0.97 ± 0.01, *n*=20, *t*-test: *p*=0.0266). Taken together, these data show reduced critical period Ca^{2+} signaling in FXS disease state inhibitory MB output neurons, another transient critical period FMRP requirement that is nearly completely resolved at maturity.

Critical period conditional control of FMRP in excitatory mPN2 neurons

Conditional control of gene function is a powerful method for developmental dissection of neural circuit formation (Bohm et al., 2010; Fore et al., 2011) and disease mechanisms (Frickenhaus et al., 2015; Herrera et al., 2013; Liu et al., 2015; Ng and Jackson, 2015). We demonstrated above that FMRP function is crucial for regulation of Ca^{2+} dynamics in both mPN2 excitatory neurons and MBON-11 inhibitory neurons only during the early-use critical period and no longer at maturity. To test this apparently restricted FMRP requirement, we next used transgenic techniques to conditionally control FMRP expression only during the critical period and specifically within only the targeted neurons. We first used the Gal80ts repressive technique (McGuire et al., 2003; Tutor et al., 2014) to temporally restore wildtype FMRP to otherwise *dfmr1* null mutants in cell-autonomous studies. In our hands, this technique provides a highly targeted method to temporally express FMRP in an otherwise completely FMRP-deficient brain (Doll and Broadie, 2015). For

mPN2 neurons, this approach involved first generating and then crossing tubP-Gal80ts; *dfmr1*^{50M}, R65G01-Gal4 to UAS-GCamp5G; *dfmr1*^{50M}, UAS-9557-3 animals. UAS-9557-3 is a genomic wildtype *dfmr1* under UAS control. All genotypes were raised at restrictive 18°C and then shifted to permissive 29°C at P4, relieving Gal80ts repression and inducing *dfmr1* expression only in mPN2 neurons (Fig. 4A). At the end of the critical period (1 dpe), brains were dissected and acutely depolarized (60mM KCl) to measure Ca^{2+} transients.

Wildtype *dfmr1* rescue of null phenotypes was tested by comparing three conditions (Fig. 4C): 1) *dfmr1* mutants containing all transgenic elements (*dfmr1*^{50M}, R65G01-Gal4>*dfmr1*^{50M}, UAS-GCamp5G; grey line), 2) *dfmr1* constitutive rescue (*dfmr1*^{50M}, R65G01-Gal4>UAS-GCamp5G; *dfmr1*^{50M}, UAS-9557-3; black line) and 3) critical period conditional rescue (tubP-Gal80ts; *dfmr1*^{50M}, R65G01-Gal4>UAS-GCamp5G; *dfmr1*^{50M}, UAS-9557-3; red line). Both constitutive (0.30 ± 0.04, n=22 neurons, Dunnett, p<0.001) and critical period-specific rescue (0.25 ± 0.04, n=25 neurons, Dunnett, p<0.001) caused a similar reduction in the peak Ca^{2+} transient compared to *dfmr1* nulls (0.52 ± 0.11, n=15 neurons, $F_{(2,57)}$=38910, p<0.001; Fig. 4C). Both depolarization-induced rescue transients are comparable to wildtype (compare Fig. 2 and 4C). Transgenic rescue led to no significant differences in time to peak (control, 9.74 ± 1.34 sec, n=15; constitutive rescue, 9.21 ± 0.90 sec, n=22; conditional rescue, 7.31 ± 0.67 sec, n=25; $F_{(2,59)}$=2.32, p=0.11, n.s.) or decay half-life (control $t_{1/2}$, 19.94 ± 2.21 sec, r^2=0.96 ± 0.01, n=14; constitutive rescue $t_{1/2}$, 27.85 ± 3.63 sec, r^2=0.96 ± 0.01, n=20; conditional rescue $t_{1/2}$, 22.53 ± 2.55 sec, r^2=0.95 ± 0.01, n=22; $F_{(2,53)}$=2.273, p=0.19, n.s.). Thus, FMRP supplied only during the critical period completely rescues functional requirements to restore Ca^{2+} signaling properties.

To complement the wildtype rescue in mPN2 neurons, cell autonomous knockdown of *dfmr1* was achieved with conditional transgenic RNA interference (RNAi). Animals were raised at the Gal80ts restrictive temperature (18°C) and then shifted to the restrictive temperature (29°C) at P4 to inactivate Gal80ts and induce *dfmr1* RNAi (Fig. 4B). Three conditions are compared (Fig. 4D); 1) control with no RNAi or Gal80ts (R65G01-Gal4>UAS-GCamp5G; grey line), 2) constitutive *dfmr1* RNAi (R65G01-Gal4>UAS-GCamp5G; *dfmr1*-RNAi, black line) and 3) conditional *dfmr1* RNAi at P4 – 1 dpe (tubP-Gal80ts; R65G01-Gal4>UAS-GCamp5G; *dfmr1*-RNAi, red line). Compared to transgenic controls, constitutive and conditional critical period *dfmr1* knockdown both resulted in highly significant increases in Ca^{2+} transient amplitude following acute K^+ depolarization (control, 0.25 ± 0.05, n=16 neurons; constitutive RNAi, 0.33 ± 0.06, n=16 neurons, Dunnett, p<0.001; conditional RNAi, 0.35 ± 0.08, n=14 neurons; Dunnett, p<0.001; $F_{(2,57)}$=5809, p<0.0001; Fig. 4D). Both knockdown strategies lead to greatly increased peak transient amplitude, thereby phenocopying 1 dpe *dfmr1* null mPN2 neurons (compare to Fig. 2). In addition, both *dfmr1* RNAi conditions led to substantial delays in time to peak (control, 5.89 ± 0.67 sec, n=16; constitutive RNAi, 8.94 ± 0.81 sec, n=14, Dunnett, p<0.05; conditional RNAi, 9.53 ± 1.14 sec, n=16, Dunnett, p<0.05; $F_{(2,43)}$=5.083, p=0.01; Fig. 4D), although transient decay properties are similar across all groups (control $t_{1/2}$, 22.95 ± 6.36 sec, r^2=0.95 ± 0.02, n=7; constitutive RNAi $t_{1/2}$, 26.41 ± 3.24 sec, r^2=0.93 ± 0.02, n=16; conditional RNAi $t_{1/2}$, 30.34 ± 5.08 sec, r^2=0.95 ± 0.01, n=13; $F_{(2,33)}$=0.5304, p=0.593). Taken together, these results show that temporally conditional and cell autonomous *dfmr1*

rescue/knockdown in mPN2 neurons within the FMRP-defined P4 – 1 dpe critical period accounts for the FMRP requirement in shaping Ca^{2+} transients, demonstrating a restricted FMRP developmental role.

Critical period dissection of FMRP function in inhibitory MBON-11 neurons

Conditional rescue and knockdown of *dfmr1* in excitatory mPN2 neurons demonstrates a precise requirement for FMRP in Ca^{2+} signaling during the critical period. We performed parallel *dfmr1* manipulations in inhibitory MBON-11 neurons to investigate the temporal requirement in these MB output cells. We first assayed constitutive vs. conditional critical period *dfmr1* rescue (Fig. 4A). Compared to *dfmr1* null mutants (*dfmr1*^{50M}, R12G04-Gal4>*dfmr1*^{50M}, UAS-GCamp5G; Fig. 4E, grey line), with a reduced Ca^{2+} transient peak amplitude at 1 dpe (0.52 ± 0.06, *n*=21 neurons), constitutive *dfmr1* rescue (*dfmr1*^{50M}, R12G04-Gal4>UAS-GCamp5G; *dfmr1*^{50M}, UAS-9557-3; Fig. 4E, black line) led to a strong restoration of wildtype peak signaling (1.05 ± 0.03, *n*=23 neurons, Dunnett, $p<0.001$). Similarly, critical period induction of FMRP (tubP-Gal80ts; *dfmr1*^{50M}, R12G04-Gal4>UAS-GCamp5G; *dfmr1*^{50M}, UAS-9557-3; Fig. 4E, red line) led to a partial, yet highly significant restoration of peak Ca^{2+} amplitude in *dfmr1* null neurons (0.69 ± 0.03, *n*=17 neurons, Dunnett, $p<0.001$; $F_{(2,57)}=40582$, $p<0.001$). Although time to peak is comparable in all groups (*dfmr1*, 6.33 ± 0.44 sec, *n*=21; constitutive rescue, 5.88 ± 0.55 sec, $p=0.53$, *n*=23; conditional rescue, 6.06 ± 0.65 sec, $p=0.72$, *n*=17; $F_{(2,49)}=0.32$, $p=0.72$, n.s.), both rescue conditions led to significant decreases in decay half-life (*dfmr1* $t_{1/2}$, 9.62 ± 0.83 sec, $r^2=0.93$ ± 0.01, *n*=21; constitutive rescue $t_{1/2}$, 7.33 ± 0.54 sec, $r^2=0.97$ ± 0.01, *n*=22, Dunnett, $p<0.05$; conditional rescue $t_{1/2}$, 6.74 ± 0.59 sec, $r^2=0.97$ ± 0.01, *n*=16, Dunnett, $p<0.05$; $F_{(2,56)}=4.998$, $p=0.0101$; Fig. 4E). Thus, *dfmr1* rescue in inhibitory MBON-11 neurons remediates Ca^{2+} transient dysfunction, albeit with conditional rescue less robust than constitutive rescue, suggesting a broader temporal requirement in this GABAergic neuron class.

To complement rescue experiments, we again employed targeted conditional RNAi (Fig. 4B). Animals were raised at the Gal80ts restrictive temperature (18°C) and then shifted to the restrictive temperature (29°C) at P4 to inactivate Gal80ts and induce *dfmr1* RNAi in MBON-11 neurons, with Ca^{2+} transients assayed at 1 dpe. Three conditions are compared (Fig. 4F): 1) transgenic control (R12G04-Gal4>UAS-GCamp5G; grey line), 2) constitutive *dfmr1* RNAi (R12G04-Gal4>UAS-GCamp5G; *dfmr1*-RNAi, black line), and 3) conditional *dfmr1* RNAi at the P4 – 1 dpe critical period (tubP-Gal80ts; R12G04-Gal4>UAS-GCamp5G; *dfmr1*-RNAi, red line). Conditional induction of *dfmr1* RNAi during the critical period is highly effective in phenocopying the *dfmr1* null mutant condition, and indeed results in a stronger effect than constitutive knockdown (Fig. 4F). Temporally targeted *dfmr1* knockdown only in the P4 – 1 dpe critical period and only in MBON-11 neurons causes a dramatic decrease in peak Ca^{2+} transient amplitude (0.41 ± 0.09, *n*=10 neurons, Dunnett, $p<0.001$) compared to controls (1.05 ± 0.10, *n*=15 neurons; $F_{(2,57)}=40268$, $p<0.001$; Fig. 4F). Constitutive *dfmr1* knockdown of *dfmr1* also causes a clear and significant reduction in peak Ca^{2+} transient amplitude (0.73 ± 0.09, *n*=21 neurons, Dunnett, $p<0.001$; Fig. 4F). We noted a slight difference in the relative time to peak Ca^{2+} influx in the conditional knockdown condition (control, 5.90 ± 0.83 sec, *n*=15 neurons; constitutive

RNAi, 6.15 ± 0.64 sec, n=21, Dunnett, p>0.05; conditional RNAi, 9.44 ± 1.57 sec, n=10, Dunnett, p<0.05; $F_{(2,43)}$=6.935, p=0.0025; Fig. 4F). Finally, decay half-life was not significantly different across all groups, despite a trend toward an extended decay in the conditional knockdown (control $t_{1/2}$, 7.20 ± 0.79 sec, r^2=0.97 ± 0.01, n=19; constitutive RNAi $t_{1/2}$, 6.98 ± 0.72 sec, r^2=0.95 ± 0.01, n=25; conditional RNAi $t_{1/2}$, 10.13 ± 1.83 sec, r^2=0.94 ± 0.01, n=14; $F_{(2,51)}$=2.205, p=0.1199; Fig. 4F). Thus, conditional removal of FMRP during the critical period actually provides a more robust effect than constitutive loss in MBON-11 neurons, an effect that also occurs in mPN2 neurons. Taken together, these results indicate an essential and restricted FMRP requirement in shaping activity-induced Ca^{2+} transients, specifically during the early-use critical period window of development.

Optogenetic critical period stimulation alters FMRP-dependent Ca^{2+} transients

Previous work has revealed that FMRP is required for activity-dependent changes in MB circuit architecture and synaptic connectivity during the early-use critical period (Doll and Broadie, 2015; Tessier and Broadie, 2008). To test whether developmental activity induces changes in Ca^{2+} signaling dynamics, we co-expressed the depolarizing UAS-channelrhodopsin (ChR2) channel along with the UAS-GCamp5G [Ca^{2+}] reporter in both excitatory input mPN2 and inhibitory output MBON-11 neurons, exposed newly-eclosed flies to a stimulating light paradigm (470 nm illumination of 20 ms pulses at 5 Hz for 24 hours) during the first day critical period following eclosion, and then performed fluorescent Ca^{2+} recordings as above. To assay mPN2 neurons, transgenic control (R65G01-Gal4>UAS-ChR2(H134R)-mCherry; UAS-GCamp5G) and *dfmr1* null mutant (*dfmr1*^{50M}, R65G01-Gal4>UAS-ChR2(H134R)-mCherry; *dfmr1*^{50M}, UAS-GCamp5G) animals were raised on either EtOH vehicle or the essential ChR2 cofactor, all-trans retinal (ATR; Ataman et al., 2008; Schroll et al., 2006). ChR2 expression was verified (Fig. 5A, red) prior to GCamp5G reporter recording (Fig. 5A, green) in individually identified neurons. A summary of the results is shown in Figure 5.

Critical period stimulation of excitatory mPN2 neurons dramatically elevates Ca^{2+} peak amplitude above vehicle control neurons ($WT^{vehicle}$, 0.18 ± 0.04, n=17 neurons; WT^{ATR}, 0.33 ± 0.06, n=18 neurons, t-test, p=9.20E-20; Fig. 5B). This amplitude change is not accompanied by a change in time to peak ($WT^{vehicle}$, 9.88 ± 0.69 sec, n=17; WT^{ATR}, 10.43 ± 0.95 sec, n=18, t-test, p=0.65, n.s.) or decay half-life ($WT^{vehicle}$ $t_{1/2}$, 43.99 ± 8.99 sec, r^2=0.92 ± 0.02, n=11; WT^{ATR} $t_{1/2}$, 40.49 ± 8.10 sec, r^2=0.92 ± 0.04, n=18, t-test, p=0.78, n.s.). Importantly, this single cell-targeted stimulation during the critical period phenocopies Ca^{2+} transients in *dfmr1* null mPN2 neurons at 1 dpe (compare to Fig. 2). Our previous work showed that *dfmr1* null mPN2 neurons lack a morphological response to developmental optogenetic manipulations (Doll and Broadie, 2015). Consistently, critical period stimulation of *dfmr1* null mPN2 neurons did not significantly affect depolarization-induced Ca^{2+} peak amplitude (*dfmr1*^{vehicle}, 0.41 ± 0.08, n=18 neurons; *dfmr1*^{ATR}, 0.38 ± 0.07, n=14 neurons, t-test, p=0.12, n.s.; Fig. 5C), time to peak (*dfmr1*^{vehicle}, 11.55 ± 1.00 sec, n=18; *dfmr1*^{ATR}, 10.92 ± 1.11 sec, n=14, t-test, p=0.68, n.s.) or half-life decay (*dfmr1*^{vehicle} $t_{1/2}$, 21.79 ± 2.7 sec, r^2=0.95 ± 0.02, n=18; *dfmr1*^{ATR} $t_{1/2}$, 27.36 ± 5.72 sec, r^2, 0.93 ± 0.03, n=13, t-test, p=0.35, n.s.). Thus, FMRP is absolutely required for activity-dependent

developmental shifts in Ca^{2+} signaling dynamics, providing evidence that FMRP acts as an essential activity sensor during critical period development.

We next tested the activity-dependent requirements for FMRP in shaping critical period Ca^{2+} signaling in inhibitory MBON-11 neurons (Fig. 6). For MBON-11, the four experimental groups were wildtype control (R12G04-Gal4>UAS-ChR2(H134R)-mCherry; UAS-GCamp5G) and *dfmr1* null (*dfmr1*^{50M}, R12G04-Gal4>UAS-ChR2(H134R)-mCherry; *dfmr1*^{50M}, UAS-GCamp5G) raised on EtOH vehicle or ATR-supplemented food. GCamp5G (Fig. 6A, green) and ChR2 (Fig. 6A, red) expression was verified in individual MBON-11 neurons. All four genotypes were exposed to 5 Hz blue light stimulation for 24 hours, with depolarization-induced Ca^{2+} transients assayed at the 1 dpe critical period (Fig. 6B,C). As in mPN2, stimulated MBON-11 neurons show a significant increase in peak Ca^{2+} transient amplitude ($WT^{vehicle}$, 0.82 ± 0.11, *n*=20 neurons; WT^{ATR}, 1.09 ± 0.16, *n*=19 neurons, *t*-test, *p*=7.58E-10; Fig. 6B), with no impact on time to peak ($WT^{vehicle}$, 6.70 ± 0.52 sec, *n*=20; WT^{ATR}, 6.22 ± 0.49 sec, *n*=19, *t*-test, *p*=0.51, n.s.; Fig. 6B) or decay half-life ($WT^{vehicle}$ $t_{1/2}$, 7.36 ± 0.49 sec, r^2=0.97 ± 0.01, *n*=20; WT^{ATR} $t_{1/2}$, 8.44 ± 0.97 sec, r^2=0.95 ± 0.01, *n*=19, *t*-test, *p*=0.32, n.s.). In sharp contrast, *dfmr1* null neurons are not susceptible to developmental activity modulation (compare Figs. 6B and 6C), as *dfmr1* mutants do not exhibit any activity-dependent increase in Ca^{2+} peak amplitude (*dfmr1*^{vehicle}, 0.62 ± 0.09, *n*=21 neurons; *dfmr1*^{ATR}, 0.57 ± 0.08, *n*=15 neurons, *t*-test, *p*=0.098; Fig. 6C) or decay half-life (*dfmr1*^{vehicle} $t_{1/2}$, 6.27 ± 0.37 sec, r^2=0.94 ± 0.01, *n*=21; *dfmr1*^{ATR} $t_{1/2}$, 6.64±0.56 sec, r^2=0.97±0.01, *n*=15, *t*-test, *p*=0.57; Fig. 6C). However, there is an increase in time to peak (*dfmr1*^{vehicle}, 5.20 ± 0.51 sec, *n*=21; *dfmr1*^{ATR} $t_{1/2}$, 10.02 ± 1.26 sec, *n*=15, *t*-test, *p*=0.00036; Fig. 6C), an effect unique to this experimental paradigm. Thus, activity-dependent changes in Ca^{2+} signaling are again absent in *dfmr1* null neurons, although we cannot rule out a stimulation-induced effect on broader timescale Ca^{2+} transients in *dfmr1* null MBON-11 neurons. Taken together, critical period stimulation of both neuron classes increases Ca^{2+} signals following depolarization, and this developmental change is completely dependent on FMRP.

Discussion

Neuron type-specific FMRP critical period requirements

The question of whether Fragile X syndrome (FXS) is a neurodevelopmental disease, a disease of continuous neural plasticity dysfunction, or some combination, is a question of paramount importance in designing effective disease interventions. The determination requires precise methods to dissect temporal requirements within defined neural circuitry. This study employs precisely-targeted transgenic drivers (Jenett et al., 2012) to introduce a [Ca^{2+}] reporter (GCamp5G) (Akerboom et al., 2012; Kirkhart and Scott, 2015) and optogenetic channelrhodopsin (ChR2) (Dani et al., 2014) into individually-identified excitatory input and inhibitory output neurons in the well-mapped MB learning/memory circuit (Tanaka et al., 2012; Tanaka et al., 2008). We previously discovered an early-use MB critical period defined by peak FMRP expression, in which FMRP loss prevents detection of sensory activity that shapes synaptic connectivity (Tessier and Broadie, 2008). More recently, we discovered excitatory input (mPN2) and inhibitory output (MBON-11) neurons

display activity-dependent bidirectional responses to depolarizing and hyperpolarizing optogenetic manipulation, only within the FMRP-defined critical period and wholly dependent on FMRP, shaping synaptic connectivity (Doll and Broadie, 2015). We show here that FMRP bidirectionally regulates critical period calcium signaling in these two neuron classes: excitatory input neurons exhibit elevated depolarization-induced transients and inhibitory output neurons display reduced transients in *dfmr1* mutants. These results reveal a novel critical period-specific mechanism supporting the E:I imbalance hypothesis of FXS (Gatto et al., 2014).

It is well established that neural circuit optimization occurs via activity-dependent changes during restricted early-use temporal windows (Hensch, 2004; Holtmaat and Svoboda, 2009). A rich history of altered neural architecture in FXS (Irwin et al., 2001; Zhang et al., 2001), and recent functional dissections demonstrate that structural defects are coupled with changes in neural excitability (Brager and Johnston, 2014). Importantly, mouse FXS models have also revealed essential roles for FMRP during critical period functional development. These include a pronounced developmental delay in excitatory somatosensory cortex (Harlow et al., 2010; Till et al., 2012), delayed depolarization-to-hyperpolarization switch in GABAergic transmission (He et al., 2014), and critical period-specific neural circuit hyperexcitation (Goncalves et al., 2013; Zhang et al., 2014). These pioneering studies of critical period refinement have provided the baseline for understanding the impact of FMRP on critical period neural circuit functional refinement, particularly in establishing and maintaining the proper excitatory-inhibitory balance (Contractor et al., 2015; Meredith, 2015).

In the *Drosophila* MB circuit, FMRP suppresses calcium signaling in excitatory input mPN2 neurons, but enhances calcium signaling in inhibitory output MBON-11 neurons (compare Figures 2 and 3). These opposing roles for FMRP occur in starkly contrasting neuron classes: excitatory cholinergic projection neurons carry olfactory sensory input (Iniguez et al., 2013), and inhibitory GABAergic MBON-11 neurons (Aso et al., 2014a) maintain aversive memory for both olfactory and visual modalities (Aso et al., 2014b). Importantly, FXS has been characterized as a disease of E:I imbalance, with increased excitation and decreased inhibition (Gibson et al., 2008). This study provides additional evidence supporting this theory, with opposite calcium signaling defects in individually-identified excitatory vs. inhibitory neurons within the same learning/memory circuit. Although we cannot rule out a maintained role for FMRP at maturity, the defects in both neuron classes are far more pronounced during the critical period of initial sensory input. Most strikingly, both *dfmr1* null neuron classes fail to undergo the dramatic developmental changes in calcium signaling that occur in wildtype animals. Conditional *dfmr1* manipulations (cell autonomous rescue and RNAi) confirm the critical period specific FMRP requirement. However, we were surprised to find more robust *dfmr1* knockdown effects within this transient period, compared to constitutive *dfmr1* knockdown in both neuron classes. This may suggest that constitutive knockdown generates nonspecific effects, such as compensation due to RNAi expression in these neurons throughout development. Conditional critical period *dfmr1* rescue provides a nearly complete restoration of calcium signaling in excitatory mPN2 neurons, but only a partial remediation of *dfmr1* defects in

inhibitory MBON-11 neurons. This may suggest that inhibitory neurons require a broader period of FMRP function during development, which may not be surprising given the persistent reduction in inhibitory signaling in this FXS disease model (Gatto et al., 2014).

FMRP control of calcium signaling during the critical period

How and why might FMRP mediate calcium signaling downstream of activity during critical period development? As an essential component of neuronal excitability, calcium influx and subsequent regulation represents a prime target for FMRP function (Tessier and Broadie, 2012). We postulate that impaired critical period calcium regulation may underlie formation of the inappropriate neural architecture and synaptic connectivity characterizing the FXS disease state (Lohmann, 2009; Tessier and Broadie, 2008; Tessier and Broadie, 2011). These functional defects may be rooted in defects in calcium buffering capacity caused by the loss of calcium-binding proteins (e.g. calmodulin and calbindin) in *dfmr1* null mutants (Tessier and Broadie, 2011). Consistently, mutations in calmodulin and calbindin lead to altered calcium transients in multiple neuronal contexts (Arredondo et al., 1998; Barski et al., 2003). It is also possible that FMRP differentially regulates calcium release from intracellular stores in a neuron type-specific manner (Tessier and Broadie, 2011). Depolarization-dependent calcium influx can occur from the outside, from calcium store organelles within the neuron, or from a combination of both, and we have previously established that FMRP is involved in calcium mobilization from both pathways in *Drosophila* brain MB neurons (Tessier and Broadie, 2011). Importantly, calcium can regulate the structural (Lohmann et al., 2005; Lohmann and Wong, 2005) and functional (Lisman et al., 2002) adaptations necessary for synaptic specificity, and defective calcium signaling may underlie multiple autism phenotypes (Krey and Dolmetsch, 2007).

The direct binding and regulation of voltage-gated Ca^{2+} and K^+ channels by FMRP represents an intriguing mechanism for the developmental maturation of circuits. A proper developmental analysis would need to include a temporal survey of channel expression in the FXS disease state, as well as roles for direct binding of FMRP to multiple classes of voltage-gated channels. For example, FMRP is capable of regulating both expression and degradation of $Ca_V2.2$ channels (Ferron et al., 2014), thereby providing both direct and indirect regulatory roles. Interestingly, Ca^{2+} channels and sensors undergo strong developmental shifts in expression and spatial organization, for example in the calyx of Held (Fedchyshyn and Wang, 2005), including developmental alterations in the type of channels expressed following initial sensory onset (Alamilla and Gillespie, 2013). Likewise, the density of presynaptic K^+ channels increases during late brain development, which correlates with shorter action potential duration (Nakamura and Takahashi, 2007). FMRP has been shown to maintain activity-dependent tonotopic $K_V3.1b$ expression gradients, with FMRP loss causing flattened tonotopicity and reduced K^+ currents (Strumbos et al., 2010). Importantly, FMRP directly binds Na^+-gated KCNT1 and Ca^{2+}-gated BK K^+ channel classes, which serve to repolarize the membrane following activity (Bean, 2007; Brown et al., 2010; Deng et al., 2013; Kim and Kaczmarek, 2014). The use of targeted *dfmr1* mutations to dissect RNA-binding translational regulation and channel-binding FMRP properties may allow us to begin to dissect these potential developmental mechanisms. For example, the newly described *dfmr1* R138Q mutation disrupts BK channel binding without

affecting translational repressive roles (Myrick et al., 2015). With such an array of regulatory capacities, FMRP modulation of channel expression and function will need to be explored both in the context of activity initiation through voltage-gated Ca^{2+} channels and activity termination via voltage-gated K^{+} channels, both of which could contribute to calcium signaling defects in the FXS disease state.

Optogenetic manipulations support FXS hyperexcitation theory

Combining optogenetic manipulation with precisely targeted neuron-specific transgenic drivers provides exciting new opportunities in developmental neuroscience (Honjo et al., 2012; Klapoetke et al., 2014). Use of these tools in the well-mapped *Drosophila* MB circuit is a particularly potent method to study activity-dependent neural development, especially to dissect cell autonomous requirements. Wildtype neurons respond to optogenetic stimulation during critical period development by strongly altering calcium signaling dynamics, but activity-dependent modulation is completely absent in *dfmr1* null neurons. Single cell-targeted stimulation during the critical period leads to increased depolarization-induced calcium signaling, providing evidence of an activity-dependent alteration in functional properties and an exciting proof-of-principle of the hyperexcitation theory of FXS (Bear et al., 2004; Goncalves et al., 2013). Of particular interest, critical period stimulation of wildtype excitatory mPN2 neurons generates depolarization-dependent calcium dynamics strikingly reminiscent of *dfmr1* null neurons, providing a specific illustration of the hyperexcitation theory of FXS (Gibson et al., 2008; Goncalves et al., 2013; Zhang et al., 2014). As projection neurons receive excitatory input from odorant receptor neurons (ORNs) in the antennal lobe (Vosshall and Stocker, 2007), this optogenetic hyper-excitation mimics exaggerated olfactory sensory input during circuit development. Thus, neurons are mis-tuned to inappropriate sensory input during the plasticity permissive critical period, resulting in calcium signaling impairments that closely mimic the FXS disease state.

Inhibitory GABAergic MBON-11 neurons also respond to heightened critical period stimulation with increased calcium signaling, demonstrating a similar activity-dependent response across neuron classes. However, this phenotype is specific to activity-manipulated wildtype neurons and does not phenocopy the *dfmr1* null condition. This suggests that inhibitory MBON-11 neurons may not be exposed to developmental hyperexcitation in the FXS condition, as predicted for mPN2. MBON-11 neurons receive input from MB Kenyon Cell neurons (Aso et al., 2014a), but the neurotransmission mechanism remains elusive (Henry et al., 2012), despite an established essential role in aversive memory formation (Aso et al., 2014b). Since FMRP regulates calcium dynamics in an opposite direction in this inhibitory neuron type, the hyperexcitation theory of FXS likely does not fully encompass the disease condition, which also includes hypo-inhibition as a prominent component. FMRP is known to regulate GABAergic components, in both *Drosophila* and mammals (Gatto et al., 2014; Lozano et al., 2014), and this likely provides a distinct FMRP regulatory mechanism on either end of the emerging E:I balance in the developing brain (Cea-Del Rio and Huntsman, 2014; Gibson et al., 2008). Unfortunately, the lack of activity response in *dfmr1* null neurons may limit our ability to use exogenous activity modulation to dissect morphology and function. However, *dfmr1* mutant neurons may display shifted critical periods (Harlow et al., 2010), and both the studied neuron classes possess calcium signaling

dynamics that are much more similar to wildtype at maturity. With the application of more advanced optogenetics techniques, such as CsChrimson (Klapoetke et al., 2014), ChR2-XXL (Dawydow et al., 2014) and red-shifted chloride inhibitors like Jaws (Chuong et al., 2014), we may be able to more effectively dissect structural and functional components of developing and mature circuits.

Conclusions

This study contributes key new insights to our understanding of the FMRP requirements in activity-dependent critical period neural circuit refinement. The powerful *Drosophila* genetic toolkit has allowed us for the first time to define both neuron-specific and temporal-specific FMRP requirements in depolarization calcium signaling dynamics. The key results are 1) excitatory and inhibitory neurons are misregulated in opposite directions in the absence of FMRP, and 2) there is a restricted FMRP requirement during the early-use critical period. In the FXS disease state, excitatory (E) neurons exhibit elevated activity-dependent calcium transients and inhibitory (I) output neurons display suppressed transients, supporting the E:I imbalance hypothesis of FXS. Moreover, restricted critical period stimulation increases calcium transients in wildtype, and this developmental refinement depends absolutely on FMRP. Single cell-targeted optogenetic stimulation and FMRP conditional manipulations establish cell-autonomous critical period functional refinement mechanisms within individually identified single excitatory and inhibitory neurons within a common learning/memory circuit. Future use of targeted human patient FMRP point mutations will allow us to dissect the roles of RNA-binding translational regulation and channel-binding activity regulation in the control of these critical period developmental mechanisms.

Acknowledgments

We are very grateful for the Bloomington *Drosophila* Stock Center (Indiana University), which provided essential genetic stocks used in this study. We particularly thank Leslie Griffith (Brandeis University) for the UAS-ChR2(H134R)-mCherry optogenetic line used in this study. We also thank Jenny Aguilar and Cheryl Gatto for intellectual input on this study. This work was fully supported by NIH grant R01 MH084989 to K.B.

References

Akerboom J, et al. Optimization of a GCaMP calcium indicator for neural activity imaging. J Neurosci. 2012; 32:13819–40. [PubMed: 23035093]

Alamilla J, Gillespie DC. Maturation of calcium-dependent GABA, glycine, and glutamate release in the glycinergic MNTB-LSO pathway. PLoS One. 2013; 8:e75688. [PubMed: 24069436]

Arredondo L, et al. Increased transmitter release and aberrant synapse morphology in a Drosophila calmodulin mutant. Genetics. 1998; 150:265–74. [PubMed: 9725845]

Aso Y, et al. The neuronal architecture of the mushroom body provides a logic for associative learning. Elife. 2014a; 3:e04577. [PubMed: 25535793]

Aso Y, et al. Mushroom body output neurons encode valence and guide memory-based action selection in Drosophila. Elife. 2014b; 3:e04580. [PubMed: 25535794]

Ataman B, et al. Rapid activity-dependent modifications in synaptic structure and function require bidirectional Wnt signaling. Neuron. 2008; 57:705–18. [PubMed: 18341991]

Barski JJ, et al. Calbindin in cerebellar Purkinje cells is a critical determinant of the precision of motor coordination. J Neurosci. 2003; 23:3469–77. [PubMed: 12716955]

Bean BP. The action potential in mammalian central neurons. Nat Rev Neurosci. 2007; 8:451–65. [PubMed: 17514198]

Bear MF, et al. The mGluR theory of fragile X mental retardation. Trends Neurosci. 2004; 27:370–7. [PubMed: 15219735]

Bohm RA, et al. A genetic mosaic approach for neural circuit mapping in Drosophila. Proc Natl Acad Sci U S A. 2010; 107:16378–83. [PubMed: 20810922]

Boyle L, Kaufmann WE. The behavioral phenotype of FMR1 mutations. Am J Med Genet C Semin Med Genet. 2010; 154C:469–76. [PubMed: 20981777]

Brager DH, Johnston D. Channelopathies and dendritic dysfunction in fragile X syndrome. Brain Res Bull. 2014; 103:11–7. [PubMed: 24462643]

Brown MR, et al. Fragile X mental retardation protein controls gating of the sodium-activated potassium channel Slack. Nat Neurosci. 2010; 13:819–21. [PubMed: 20512134]

Cea-Del Rio CA, Huntsman MM. The contribution of inhibitory interneurons to circuit dysfunction in Fragile X Syndrome. Front Cell Neurosci. 2014; 8:245. [PubMed: 25202236]

Chen L, et al. The fragile X mental retardation protein binds and regulates a novel class of mRNAs containing U rich target sequences. Neuroscience. 2003; 120:1005–17. [PubMed: 12927206]

Chuong AS, et al. Noninvasive optical inhibition with a red-shifted microbial rhodopsin. Nat Neurosci. 2014; 17:1123–9. [PubMed: 24997763]

Contractor A, et al. Altered Neuronal and Circuit Excitability in Fragile X Syndrome. Neuron. 2015; 87:699–715. [PubMed: 26291156]

Dani N, et al. Two protein N-acetylgalactosaminyl transferases regulate synaptic plasticity by activity-dependent regulation of integrin signaling. J Neurosci. 2014; 34:13047–65. [PubMed: 25253852]

Dawydow A, et al. Channelrhodopsin-2-XXL, a powerful optogenetic tool for low-light applications. Proc Natl Acad Sci U S A. 2014; 111:13972–7. [PubMed: 25201989]

Deng PY, et al. FMRP regulates neurotransmitter release and synaptic information transmission by modulating action potential duration via BK channels. Neuron. 2013; 77:696–711. [PubMed: 23439122]

Deng PY, et al. Abnormal presynaptic short-term plasticity and information processing in a mouse model of fragile X syndrome. J Neurosci. 2011; 31:10971–82. [PubMed: 21795546]

Doll CA, Broadie K. Impaired activity-dependent neural circuit assembly and refinement in autism spectrum disorder genetic models. Frontiers in Cellular Neuroscience. 2014; 8

Doll CA, Broadie K. Activity-dependent FMRP requirements in development of the neural circuitry of learning and memory. Development. 2015; 142:1346–56. [PubMed: 25804740]

Fedchyshyn MJ, Wang LY. Developmental transformation of the release modality at the calyx of Held synapse. J Neurosci. 2005; 25:4131–40. [PubMed: 15843616]

Ferron L, et al. Fragile X mental retardation protein controls synaptic vesicle exocytosis by modulating N-type calcium channel density. Nat Commun. 2014; 5:3628. [PubMed: 24709664]

Fiala A, Spall T. In vivo calcium imaging of brain activity in Drosophila by transgenic cameleon expression. Sci STKE. 2003; 2003:PL6. [PubMed: 12644713]

Fore TR, et al. Mapping and application of enhancer-trap flippase expression in larval and adult Drosophila CNS. J Vis Exp. 2011

Frickenhaus M, et al. Highly efficient cell-type-specific gene inactivation reveals a key function for the Drosophila FUS homolog cabeza in neurons. Sci Rep. 2015; 5:9107. [PubMed: 25772687]

Gatto CL, Broadie K. Temporal requirements of the fragile X mental retardation protein in the regulation of synaptic structure. Development. 2008; 135:2637–48. [PubMed: 18579676]

Gatto CL, Broadie K. The fragile X mental retardation protein in circadian rhythmicity and memory consolidation. Mol Neurobiol. 2009; 39:107–29. [PubMed: 19214804]

Gatto CL, Broadie K. Genetic controls balancing excitatory and inhibitory synaptogenesis in neurodevelopmental disorder models. Front Synaptic Neurosci. 2010; 2:4. [PubMed: 21423490]

Gatto CL, et al. GABAergic circuit dysfunction in the Drosophila Fragile X syndrome model. Neurobiol Dis. 2014; 65:142–59. [PubMed: 24423648]

Gibson JR, et al. Imbalance of neocortical excitation and inhibition and altered UP states reflect network hyperexcitability in the mouse model of fragile X syndrome. J Neurophysiol. 2008; 100:2615–26. [PubMed: 18784272]

Goncalves JT, et al. Circuit level defects in the developing neocortex of Fragile X mice. Nat Neurosci. 2013; 16:903–9. [PubMed: 23727819]

Gross C, et al. Fragile X mental retardation protein regulates protein expression and mRNA translation of the potassium channel Kv4.2. J Neurosci. 2011; 31:5693–8. [PubMed: 21490210]

Harlow EG, et al. Critical period plasticity is disrupted in the barrel cortex of FMR1 knockout mice. Neuron. 2010; 65:385–98. [PubMed: 20159451]

He Q, et al. The developmental switch in GABA polarity is delayed in fragile X mice. J Neurosci. 2014; 34:446–50. [PubMed: 24403144]

Henry GL, et al. Cell type-specific genomics of Drosophila neurons. Nucleic Acids Res. 2012; 40:9691–704. [PubMed: 22855560]

Hensch TK. Critical period regulation. Annu Rev Neurosci. 2004; 27:549–79. [PubMed: 15217343]

Herrera SC, et al. Tissue homeostasis in the wing disc of Drosophila melanogaster: immediate response to massive damage during development. PLoS Genet. 2013; 9:e1003446. [PubMed: 23633961]

Holtmaat A, Svoboda K. Experience-dependent structural synaptic plasticity in the mammalian brain. Nat Rev Neurosci. 2009; 10:647–58. [PubMed: 19693029]

Honjo K, et al. Optogenetic manipulation of neural circuits and behavior in Drosophila larvae. Nature protocols. 2012; 7:1470–1478. [PubMed: 22790083]

Iniguez J, et al. Cav3-type alpha1T calcium channels mediate transient calcium currents that regulate repetitive firing in Drosophila antennal lobe PNs. J Neurophysiol. 2013; 110:1490–6. [PubMed: 23864373]

Irwin SA, et al. Abnormal dendritic spine characteristics in the temporal and visual cortices of patients with fragile-X syndrome: a quantitative examination. Am J Med Genet. 2001; 98:161–7. [PubMed: 11223852]

Ito K, et al. A systematic nomenclature for the insect brain. Neuron. 2014; 81:755–65. [PubMed: 24559671]

Jenett A, et al. A GAL4-driver line resource for Drosophila neurobiology. Cell Rep. 2012; 2:991–1001. [PubMed: 23063364]

Kaeser PS, Regehr WG. Molecular mechanisms for synchronous, asynchronous, and spontaneous neurotransmitter release. Annu Rev Physiol. 2014; 76:333–63. [PubMed: 24274737]

Kim GE, Kaczmarek LK. Emerging role of the KCNT1 Slack channel in intellectual disability. Front Cell Neurosci. 2014; 8:209. [PubMed: 25120433]

Kirkhart C, Scott K. Gustatory learning and processing in the Drosophila mushroom bodies. J Neurosci. 2015; 35:5950–8. [PubMed: 25878268]

Klapoetke NC, et al. Independent optical excitation of distinct neural populations. Nat Methods. 2014; 11:338–46. [PubMed: 24509633]

Krey JF, Dolmetsch RE. Molecular mechanisms of autism: a possible role for Ca2+ signaling. Curr Opin Neurobiol. 2007; 17:112–9. [PubMed: 17275285]

Lee HY, et al. Bidirectional regulation of dendritic voltage-gated potassium channels by the fragile X mental retardation protein. Neuron. 2011; 72:630–42. [PubMed: 22099464]

Lisman J, et al. The molecular basis of CaMKII function in synaptic and behavioural memory. Nat Rev Neurosci. 2002; 3:175–90. [PubMed: 11994750]

Liu Y, et al. Serotonin and insulin-like peptides modulate leucokinin-producing neurons that affect feeding and water homeostasis in Drosophila. J Comp Neurol. 2015; 523:1840–63. [PubMed: 25732325]

Lohmann C. Calcium signaling and the development of specific neuronal connections. Prog Brain Res. 2009; 175:443–52. [PubMed: 19660672]

Lohmann C, et al. Local calcium transients regulate the spontaneous motility of dendritic filopodia. Nat Neurosci. 2005; 8:305–12. [PubMed: 15711541]

Lohmann C, Wong RO. Regulation of dendritic growth and plasticity by local and global calcium dynamics. Cell Calcium. 2005; 37:403–9. [PubMed: 15820387]

Lozano R, et al. Modulation of the GABAergic pathway for the treatment of fragile X syndrome. Neuropsychiatr Dis Treat. 2014; 10:1769–79. [PubMed: 25258535]

McGuire SE, et al. Spatiotemporal rescue of memory dysfunction in Drosophila. Science. 2003; 302:1765–8. [PubMed: 14657498]

Meredith RM. Sensitive and critical periods during neurotypical and aberrant neurodevelopment: a framework for neurodevelopmental disorders. Neurosci Biobehav Rev. 2015; 50:180–8. [PubMed: 25496903]

Myrick LK, et al. Independent role for presynaptic FMRP revealed by an FMR1 missense mutation associated with intellectual disability and seizures. Proc Natl Acad Sci U S A. 2015; 112:949–56. [PubMed: 25561520]

Nakamura Y, Takahashi T. Developmental changes in potassium currents at the rat calyx of Held presynaptic terminal. J Physiol. 2007; 581:1101–12. [PubMed: 17331991]

Ng FS, Jackson FR. The ROP vesicle release factor is required in adult Drosophila glia for normal circadian behavior. Front Cell Neurosci. 2015; 9:256. [PubMed: 26190976]

Pan L, et al. The Drosophila fragile X gene negatively regulates neuronal elaboration and synaptic differentiation. Curr Biol. 2004; 14:1863–70. [PubMed: 15498496]

Patel AB, et al. A target cell-specific role for presynaptic Fmr1 in regulating glutamate release onto neocortical fast-spiking inhibitory neurons. J Neurosci. 2013; 33:2593–604. [PubMed: 23392687]

Portera-Cailliau C. Which comes first in fragile X syndrome, dendritic spine dysgenesis or defects in circuit plasticity? Neuroscientist. 2012; 18:28–44. [PubMed: 21551076]

Pulver SR, et al. Temporal dynamics of neuronal activation by Channelrhodopsin-2 and TRPA1 determine behavioral output in Drosophila larvae. J Neurophysiol. 2009; 101:3075–88. [PubMed: 19339465]

Repicky S, Broadie K. Metabotropic glutamate receptor-mediated use-dependent down-regulation of synaptic excitability involves the fragile X mental retardation protein. J Neurophysiol. 2009; 101:672–87. [PubMed: 19036865]

Schneider CA, et al. NIH Image to ImageJ: 25 years of image analysis. Nat Methods. 2012; 9:671–5. [PubMed: 22930834]

Schroll C, et al. Light-induced activation of distinct modulatory neurons triggers appetitive or aversive learning in Drosophila larvae. Curr Biol. 2006; 16:1741–7. [PubMed: 16950113]

Strumbos JG, et al. Fragile X mental retardation protein is required for rapid experience-dependent regulation of the potassium channel Kv3.1b. J Neurosci. 2010; 30:10263–71. [PubMed: 20685971]

Tanaka NK, et al. Organization of antennal lobe-associated neurons in adult Drosophila melanogaster brain. J Comp Neurol. 2012; 520:4067–130. [PubMed: 22592945]

Tanaka NK, et al. Neuronal assemblies of the Drosophila mushroom body. J Comp Neurol. 2008; 508:711–55. [PubMed: 18395827]

Tessier CR, Broadie K. Drosophila fragile X mental retardation protein developmentally regulates activity-dependent axon pruning. Development. 2008; 135:1547–57. [PubMed: 18321984]

Tessier CR, Broadie K. The fragile X mental retardation protein developmentally regulates the strength and fidelity of calcium signaling in Drosophila mushroom body neurons. Neurobiol Dis. 2011; 41:147–59. [PubMed: 20843478]

Tessier CR, Broadie K. Molecular and genetic analysis of the Drosophila model of fragile X syndrome. Results Probl Cell Differ. 2012; 54:119–56. [PubMed: 22009350]

Till SM, et al. Altered maturation of the primary somatosensory cortex in a mouse model of fragile X syndrome. Hum Mol Genet. 2012; 21:2143–56. [PubMed: 22328088]

Tomchik SM, Davis RL. Dynamics of learning-related cAMP signaling and stimulus integration in the Drosophila olfactory pathway. Neuron. 2009; 64:510–21. [PubMed: 19945393]

Tutor AS, et al. Src64B phosphorylates Dumbfounded and regulates slit diaphragm dynamics: Drosophila as a model to study nephropathies. Development. 2014; 141:367–76. [PubMed: 24335255]

Vosshall LB, Stocker RF. Molecular architecture of smell and taste in Drosophila. Annu Rev Neurosci. 2007; 30:505–33. [PubMed: 17506643]

Wang H, et al. Ca2+/calmodulin-dependent protein kinase IV links group I metabotropic glutamate receptors to fragile X mental retardation protein in cingulate cortex. J Biol Chem. 2009; 284:18953–62. [PubMed: 19436069]

Wang T, et al. New perspectives on the biology of fragile X syndrome. Curr Opin Genet Dev. 2012; 22:256–63. [PubMed: 22382129]

Weisz ED, et al. Deciphering discord: How Drosophila research has enhanced our understanding of the importance of FMRP in different spatial and temporal contexts. Exp Neurol. 2015

Zhang Y, et al. Dendritic channelopathies contribute to neocortical and sensory hyperexcitability in Fmr1(-/y) mice. Nat Neurosci. 2014; 17:1701–9. [PubMed: 25383903]

Zhang Y, et al. Regulation of neuronal excitability by interaction of fragile X mental retardation protein with slack potassium channels. J Neurosci. 2012; 32:15318–27. [PubMed: 23115170]

Zhang YQ, et al. Drosophila fragile X-related gene regulates the MAP1B homolog Futsch to control synaptic structure and function. Cell. 2001; 107:591–603. [PubMed: 11733059]

Highlights

- Fragile X syndrome (FXS) is the leading heritable cause of autism spectrum disorders
- Imbalance between excitation (E) and inhibition (I) common in autistic brain circuits
- Opposite activity-dependent Ca^{2+} signaling defects in E vs. I neurons in a FXS model
- FXS Ca^{2+} signaling defects specific to the early-use critical period of development

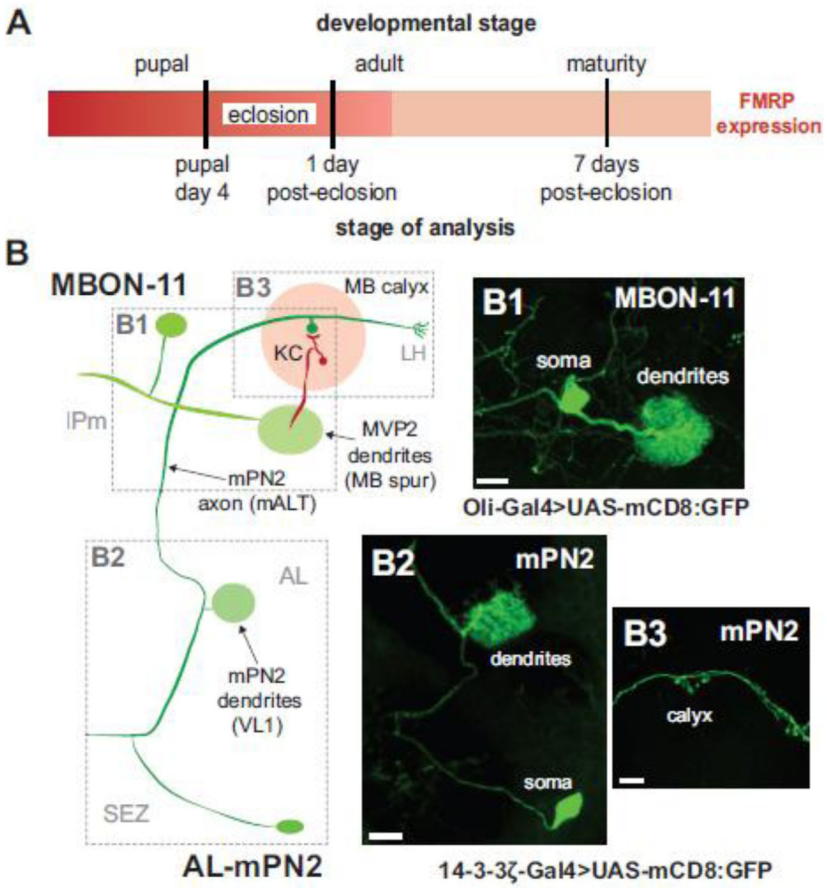

Figure 1.

Critical period manipulation of excitatory input and inhibitory output neurons of the mushroom body learning/memory circuit. **A**) Schematic illustrating developmental stages of analysis relative to the FMRP expression profile (Tessier and Broadie, 2008). **B**) Schematic depicting architecture of MB input excitatory cholinergic neuron AL-mPN2 (R65G01-Gal4 driver) and MB output inhibitory GABAergic neuron MBON-γ1pedc>α/β (MBON-11; R12G04-Gal4 driver). The membrane marker UAS-mCD8 is shown for MBON-11 (**B1**) and mPN2 (**B2**, **B3**) labeling soma, dendritic arbor and axon processes. Dashed boxes correspond to images. Abbreviations: MB, Mushroom body; AL, antennal lobe; ON, output neuron; SEZ, subesophogeal zone; IPm medial inferior protocerebrum; KC, Kenyon cell; LH, lateral horn; VL, vertical lobe; ML, medial lobe; mALT, medial antennal lobe tract; PN, projection neuron; VL1, ventrolateral glomerulus 1; AL-mPN2, antennal lobe medial projection neuron 2. Scale B1: 10μM, B2: 20μM, B3: 10μM.

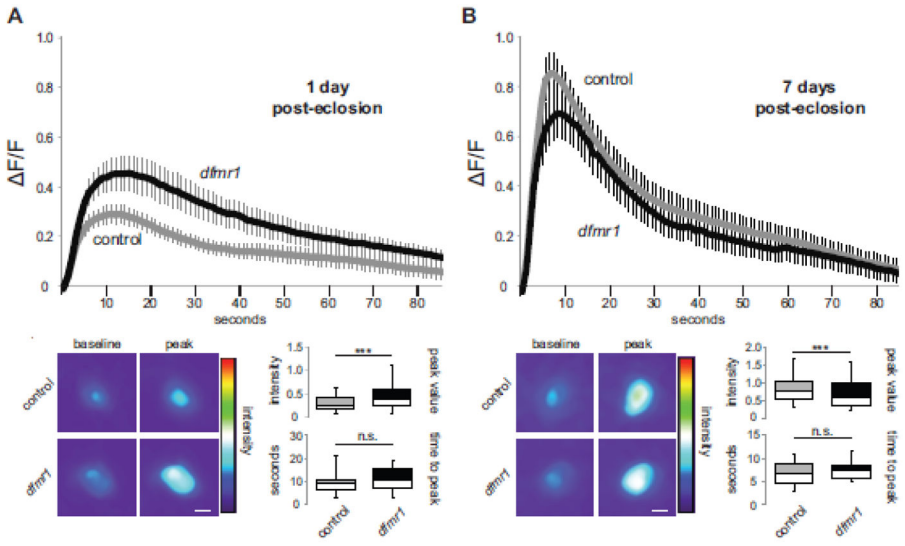

Figure 2.

Restricted critical period defect in AL-mPN2 Ca^{2+} dynamics in *dfmr1* mutants. The UAS-GCamp5G fluorescent reporter driven by R65G01-Gal4 in excitatory mPN2 input neurons to assay depolarization-induced Ca^{2+} transients in both wildtype control (w^{1118}) and *dfmr1* null mutants. Confocal fluorescent measurements done at the peak critical period of 1 day post-eclosion (**A**) compared to maturity at 7 days post-eclosion (**B**). Still frame heat map representations of baseline and peak fluorescence following acute K+ depolarization. The change of average fluorescence intensity over time (mean±SEM) is plotted on top, with histograms (minimum, median, maximum and quartiles) below depicting peak intensity and time to peak. $n^{\text{WT-1dpe}}$=19, $n^{dfmr1\text{-1dpe}}$=17, $n^{\text{WT-7dpe}}$=22, $n^{dfmr1\text{-7dpe}}$=18. Statistical significance indicated as ***p<0.001 or not significant (n.s.). Scale bars: 10μm.

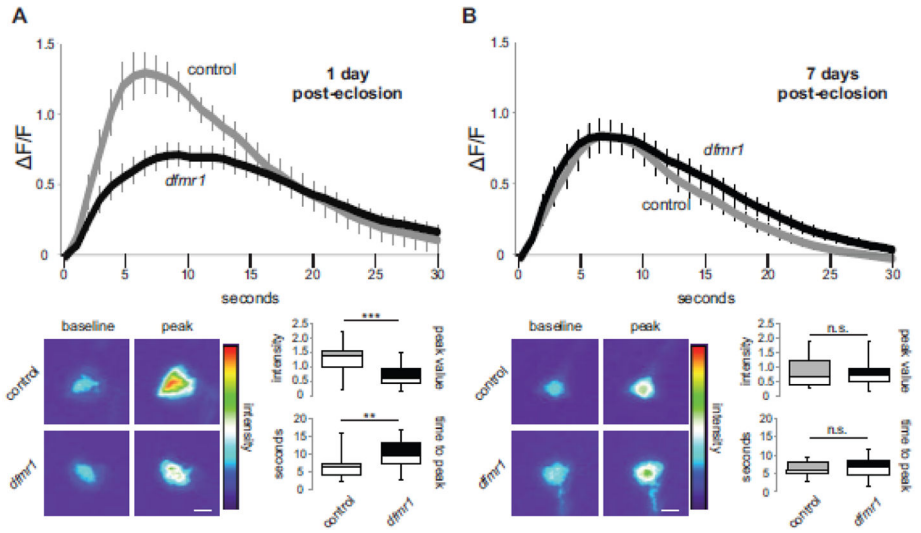

Figure 3.

Opposite critical period defect in MBON-11 Ca^{2+} dynamics in *dfmr1* mutants. UAS-GCamp5G fluorescent reporter targeted by the R12G04-Gal4 driver to inhibitory MBON-11 output neurons to assay depolarization-induced Ca^{2+} transients in wildtype control (w^{1118}) and *dfmr1* null mutants. Measurements at the 1 day post-eclosion critical period (**A**) compared to maturity at 7 days post-eclosion (**B**). Representative heat maps show baseline and peak fluorescence following acute K+ depolarization. The change of average fluorescence intensity over time (mean±SEM) is plotted on top, with histograms (minimum, median, maximum and quartiles) below depicting peak intensity and time to peak. $n^{\text{WT-1dpe}}$=20, $n^{dfmr1\text{-1dpe}}$=16, $n^{\text{WT-7dpe}}$=22, $n^{dfmr1\text{-7dpe}}$=23. Statistical significance indicated as **p<0.01, ***p<0.001 or not significant (n.s.). Scale bars: 10μm.

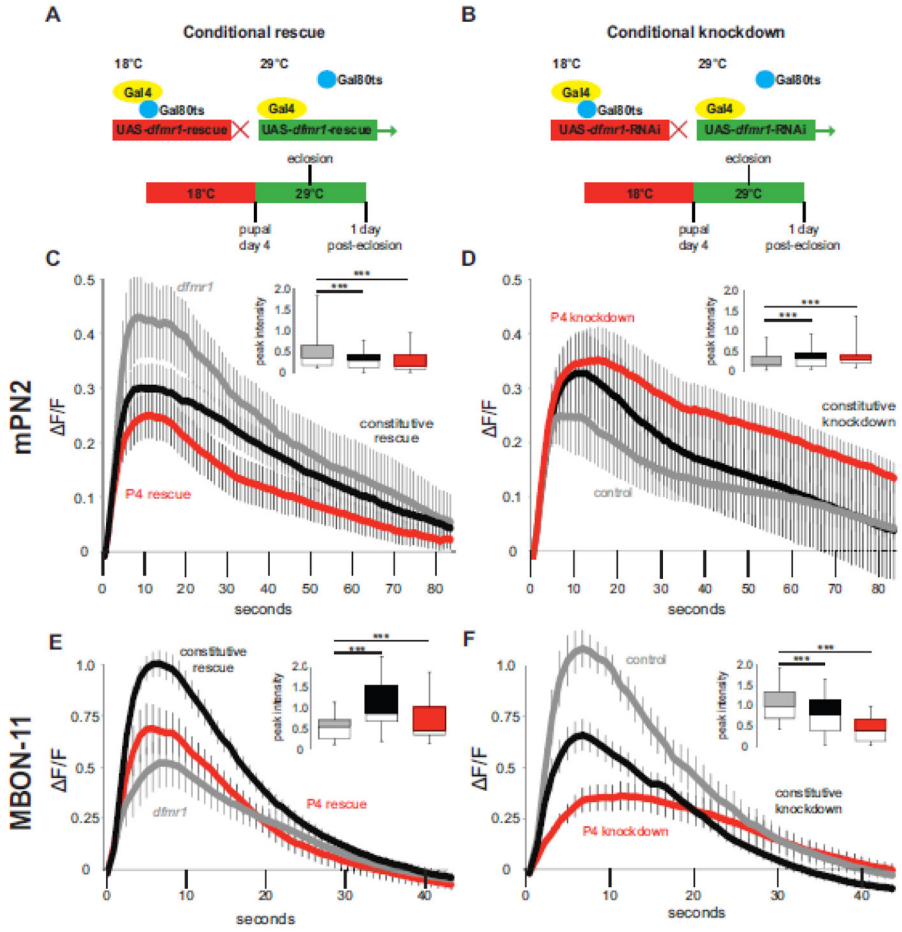

Figure 4.

Conditional *dfmr1* rescue/removal shows restricted critical period requirement. Gal80ts repressive paradigm for conditionally *dfmr1* rescue (**A**) and knockdown (**B**) during critical period development for both excitatory input mPN2 and inhibitory output MBON-11 neurons. Animals raised at 18°C permissive temperature (Gal80 active, Gal4 inactive, red) until pupal day 4 (P4), then shifted to 29°C restrictive temperature (Gal80 inactive, Gal4 active, green) until 1 day post-eclosion (1 dpe). (**C–F**) K^+ depolarization-induced Ca^{2+} transient GCamp5G fluorescence changes for genetic controls (grey line), constitutively active rescue/RNAi (black line), and conditional Gal80ts rescue/RNAi (red line). AL-mPN2 *dfmr1* critical period rescue (*dfmr1* control *n*=15, constitutive rescue *n*=22, conditional rescue *n*=25) (**C**) and RNAi knockdown (WT control *n*=16, constitutive RNAi *n*=16, conditional RNAi *n*=14) (**D**) shows restricted temporal FMRP requirement. Parallel, MBON-11 critical period rescue (*dfmr1* control *n*=21, constitutive rescue *n*=23, conditional rescue *n*=17) (**E**) and removal (WT control *n*=15, constitutive RNAi *n*=21, conditional RNAi *n*=10) (**F**) of *dfmr1* shows similar results. Each plot represents the change of average fluorescence intensity over time (mean±SEM), and includes an inset peak intensity histogram (minimum, median, maximum and quartiles). Significance determined by one-way ANOVA and indicated as ***p<0.001 or not significant (n.s.).

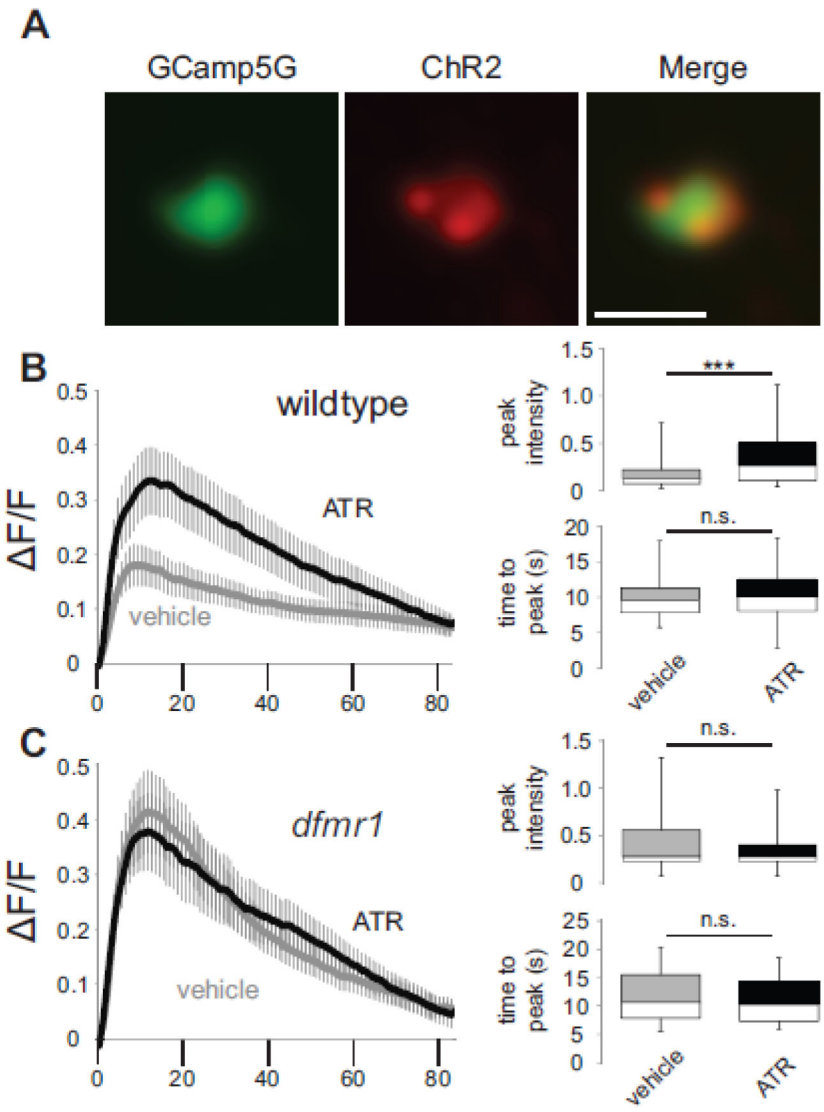

Figure 5.

Critical period stimulation of mPN2 reveals FMRP-dependent Ca^{2+} dynamics. (**A**) Co-expression of UAS-GCamp5G Ca^{2+} reporter (green) and UAS-ChR2-H134R-mCherry optogenetic channel (red) driven by R65G01-Gal4 targeted to excitatory MB input mPN2 neurons. K^{+} depolarization-induced Ca^{2+} transients following 24 hours of blue light stimulation (5Hz, 20ms) in animals fed either vehicle alone or the all-trans retinal (ATR) essential cofactor for optogenetic stimulation in wildtype control (**B**) or *dfmr1* null mutants (**C**). Left: Change of average fluorescence intensity over time (F/F; mean±SEM). Right: Histograms (minimum, median, maximum and quartiles) depicting fluorescence peak intensity and time to peak fluorescence. $WT^{vehicle}$ *n*=17, WT^{ATR} *n*=18, $dfmr1^{vehicle}$ *n*=18, $dfmr1^{ATR}$ *n*=14. Statistical significance determined via unpaired, two-tailed t-tests indicated as ***p<0.001 or not significant (n.s.). Scale bar: 0.5μm.

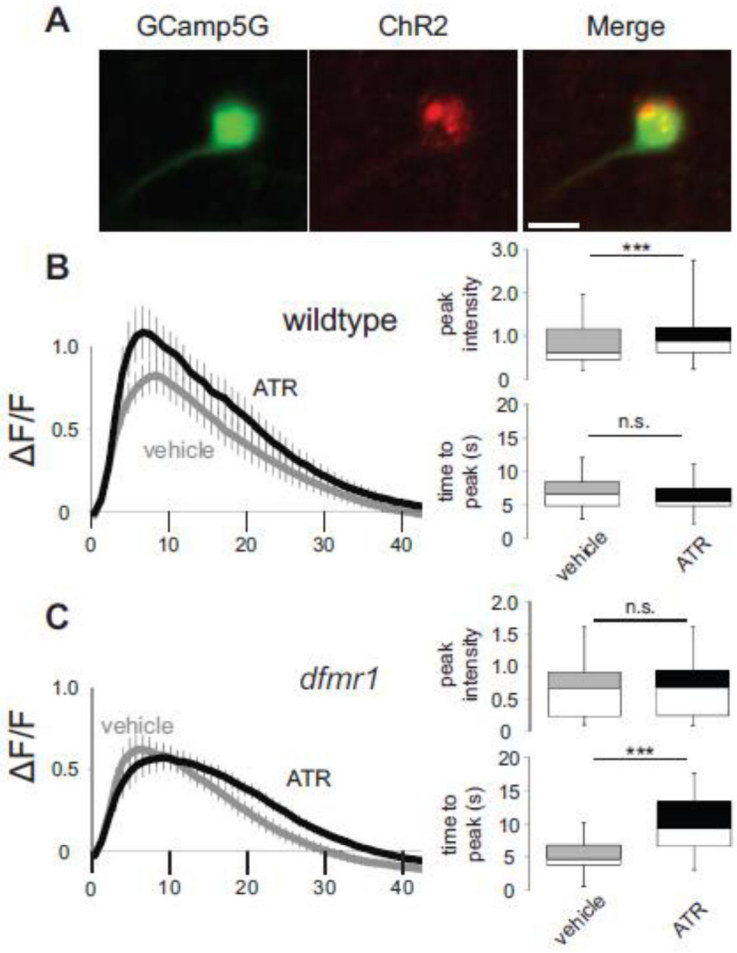

Figure 6.

Critical period MBON-11 stimulation shows FMRP-dependent Ca^{2+} dynamics. (**A**) Dual expression of the UAS-GCamp5G Ca^{2+} reporter (green) and the UAS-ChR2-H134R-mCherry optogenetic channel (red) under control of the R12G04-Gal4 driver selectively targeted to inhibitory output MBON-11 neurons. K^+ depolarization-induced Ca^{2+} transients following 24 hours of blue light stimulation (5Hz, 20ms) in animals fed either vehicle or all-trans retinal (ATR) for optogenetic stimulation in wildtype control (**B**) and *dfmr1* null mutants (**C**). The change of average fluorescence intensity (mean±SEM) following acute K^+ depolarization is shown on the left, with histograms on the right depicting the GCamp5G Ca^{2+} reporter fluorescence peak intensity and time to peak (minimum, median, maximum and quartiles). $WT^{vehicle}$ n=20, WT^{ATR} n=19, $dfmr1^{vehicle}$ n=21, $dfmr1^{ATR}$ n=15. Statistical significance determined via unpaired, two-tailed t-tests indicated as ***p<0.001 or not significant (n.s.). Scale bar: 10μm.